Journal of Environmental Chemical Engineering 6 (2018) 4961–4969

Contents lists available at ScienceDirect

Journal of Environmental Chemical Engineering

journal homepage: www.elsevier.com/locate/jece

Adsorption performance toward organic pollutants, odour control and antimicrobial activities of one Ag-based coordination polymer

Ang Liu[a], Chang-Zheng Wang[a], Chun Chu[a], Hong-Yu Chu[a], Xi Chen[a], Ao-Fei Du[a], Jing Mao[a], Weiwei Zheng[b], Chong-Chen Wang[a,*]

[a] Beijing Key Laboratory of Functional Materials for Building Structure and Environment Remediation, Beijing University of Civil Engineering and Architecture, Beijing, 100044, China
[b] Chemistry, Syracuse University, Syracuse, NY, 13244, United States

ARTICLE INFO

Keywords:
Coordination polymer
Organic pollutant
Adsorption
Odour control
Antimicrobial activity

ABSTRACT

A silver-based coordination polymer $[Ag_2(idca)(H_2O)_2]$ (**BUC-16**), had been successfully prepared and used as efficient adsorbent to perform adsorption toward organic pollutants like promethazine hydrochlorine (PMH, 1395 mg g^{-1}), sulfamethoxazole (SMX, 675 mg g^{-1}), methylene blue (MB, 1317 mg g^{-1}) in simulated wastewater. The slow-release of Ag^+ ions from **BUC-16** leads to its efficient and long-term antimicrobial and alga-inhibiting (odour control) activities. This is the first study on alga-inhibiting properties of coordination polymer, to the best of our knowledge. In vitro cytotoxicity (NIH-3T3 cells) test showed that **BUC-16** has lower cell toxicity, implying its good biocompatibility.

1. Introduction

Coordination polymers (CPs) including metal-organic frameworks (MOFs) are new class of inorganic-organic hybrid materials with diverse compositions, easily tailored structures, ultrahigh surfaces and active sites [1–4]. Therefore, CPs have many potential applications, including catalysis [5], photocatalysis [6–10], anti-microbial [11,12], gas storage & separation [13,14], pollutants adsorption [12,15–18], sensing [19], fluorescence [20], magnetism [21], drug delivery [22], and so on [1,23,24].

Recently, some CPs including MOFs were used as adsorbents to conduct efficient removal of hazardous pollutants such as heavy metals [18,25,26] and organic pollutants [12,16,17,27–32] due to their striking characteristics of cavities with regular size and shape, well-defined channels, surface charges, and rich active sites. Some CPs can be used to conduct selective adsorption and efficient separation of organic pollutants with different charges by matrix resulting from their electronic interactions and/or guest-guest exchange interactions [12,16,17]. Furthermore, some CPs could act as reservoirs to slowly release metal ions like Ag^+, Zn^{2+}, Cu^{2+}/Cu^+, which exhibited excellent antibacterial performance because the released metal ions could be used to diffuse into the bacterial membrane and destroy the cell membrane proteins [12,33]. In our recent studies, silver-based CPs presented outstanding adsorptive performances toward serval organic pollutants and excellent antibacterial activities [12].

To extend the capacity of metal-based CPs in the treatment of black-odour water, in this work, we present a new silver-based coordination polymer to achieve outstanding adsorption performances toward organic pollutants inluding PPCPs and organic dyes, remarkable alga-inhibiting (odour control) activity along with antimicrobial property inhibitating *E. Coli*. This is the first report on the odour (β-cyclocitral) control using coordination polymer, to the best of our knowledge.

2. Experimental

2.1. Materials and instruments

All chemicals and solvents were commercially available and used directly without any further treatment. *Escherichia coli* (CICC 23429) and M. aeruginosa (FACHB-905) were purchased from the China Centre of Industrial Culture Collection (Beijing, China) and Institute of Hydrobiology (Chinese Academy of Sciences, Wuhan, China), respectively. NIH-3T3 (mouse embryo fibroblast) cell lines were purchased from Institute of Biochemistry and Cell Biology (Shanghai, China).

Fourier Transform infrared spectra (FTIR) in the region of 400–4000 cm^{-1} were recorded on a Nicolet 6700 FTIR spectrophotometer with KBr pellets. Powder X-ray diffraction (XRD) patterns were recorded using a Dandonghaoyuan DX-2700B diffractometer with

* Corresponding author.
E-mail address: chongchenwang@126.com (C.-C. Wang).

https://doi.org/10.1016/j.jece.2018.07.035
Received 13 June 2018; Received in revised form 18 July 2018; Accepted 20 July 2018
Available online 21 July 2018

Cu Kα radiation. The change of bacteria and count of M. aeruginosa were observed with the aid of Axio Imager A2 microscope (Carl Zeiss, Germany). The released Ag^+ amount was determined on ICAP 7000 inductively coupled plasma optical emission spectrometer (ICP-OES), and the analysis parameters were listed in Table S1. The morphological changes of the bacteria were observed by Hitachi-HT7700 transmission electron microscopy and Hitachi TM3030 plus scanning electron microscopy. The surface charge of the particles was assessed by zeta potential measurements using the Malvern zeta sizer Nano ZS and by applying the field strength of 20 V cm^{-1}.

Single-crystal X-ray diffraction data collection for **BUC-16** were performed with a Bruker Smart 1000 CCD area detector diffractometer with graphite-monochromatized MoKα radiation (λ = 0.71073 Å) using *φ*-*ω* mode at 298(2) K. The SMART software [34] was used for data collection and the SAINT software for data extraction. Empirical absorption corrections were performed with the SADABS program [35]. The structures were solved by direct methods (SHELXS-97) and refined by full-matrix-least squares techniques on F^2 with anisotropic thermal parameters for all of the non-hydrogen atoms (SHELXL-97). All hydrogen atoms were located by Fourier difference synthesis and geometrical analysis. These hydrogen atoms were assigned to ride on their respective parent atoms. All structural calculations were carried out using the SHELX-97 program package. Crystallographic data and structural refinements for **BUC-16** were summarized in Tables S2 and S3. Selected bond lengths and angles were listed in Table S4.

A Laspec Alpha-1860 spectrometer was used to monitor the methyl orange (MO), Basic Brown 1 (BB-1), methylene blue (MB) and rhodamine B (RhB) concentration changes by the maximum absorbance at 463, 457, 664 and 552 nm, respectively.

The sulfamethoxazole (SMX) and promethazine hydrochlorine (PMH) concentrations were measured by using Waters UPLC (ACQUITY, USA) apparatus (photodiode array detector 996, auto sampler 717, and controller 600) equipped with Millennium software. An ACQUITY UPLC BEH C18 column (1.7 μm, 150 mm × 2.1 mm) was adopted as reverse-phase column. As to the determination of promethazine hydrochlorine, a mixture of water and MeOH (55:45) adjusted at pH = 2.7 with acetic acid was the mobile phase, which was isocratically delivered by a pump at a flow rate of 1 mL min^{-1}. The wavelength of the UV absorbance detector was 254 nm (Fig. S1a). To conduct determination of sulfamethoxazole concentration, the mobile phase was a mixture of water and acetonitrile (60:40) adjusted at pH = 3 with phosphoric acid, which was isocratically delivered by a pump at a flow rate of 1 mL min^{-1}. The wavelength of the UV absorbance detector was 270 nm (Fig. S1b). Mass spectra were obtained on a Micromass VG-Platform.

The analysis of *β*-cyclocitral was performed by GC–MS QP2010 PLUS system (Shimadzu, Japan), operated at 70 eV electron impact [36]. Data acquisition and analysis were performed on the GC–MS Real-Time Analysis and GCMS Postrun Analysis software (Shimadzu), respectively. The separation was achieved on a fused silica capillary column coated with a 5% diphenyl and 95% dimethyl polysiloxane stationary phase (Rxi-5Sil MS, 30 m × 0.25 mm id, 0.25 μm; Restek, Bellefonte, PA, USA). Helium gas with purity > 99.999% was used as the GC carrier gas at a flow rate of 37.5 cm s^{-1} in the constant linear velocity mode. The extracts of 1.0 μL were injected in the spitless mode for 1.0 min at an injection temperature of 270 ℃ with a solvent delay of 5 min. Subsequently, the GC column was heated to 160 ℃ for 2 min initially, and then the temperature was programmed to 255℃ at 20 ℃ min^{-1} (held for 4 min), to 260 ℃ at 10 ℃ min^{-1} (held for 5 min), and finally to 270 ℃ at 10 ℃ min^{-1} (held for 3 min). The temperature of the transfer line and the ion source was 250 and 200 ℃, respectively. The retention time and the fragment ions were identified by injecting the multicompound standard in full-scan mode (*m/z* being 50–500). Ion peaks including one for quantitation and two for qualification were monitored for each PYR based on the full-scan results. The retention time (16.658 min) and single ion monitoring (SIM) parameters (94, 124, 151, 137) for each analyte are listed in Fig. S1c. Quantification was performed by calculating the absolute peak areas in SIM mode (Fig. S1c).

2.2. Synthesis of $[Ag_2(idca)(H_2O)_2]$ (BUC-16)

The ammonia solution (125 mL, 0.5 mol L^{-1}) of $AgNO_3$ (1.25 mmol, 0.21 g) and the ammonia solution of 4,5-imidazoledicarboxylic acid (H_2idca, 1.25 mmol, 0.20 g) were mixed dropwise, and the mixture was stirred for 15 min, then allowed to evaporate slowly at room temperature in the dark. Block-like white crystals of $[Ag_2(idca)(H_2O)_2]$ (**BUC-16**) were obtained after 2 weeks (yield 87% based on $AgNO_3$). Anal. Calcd. for $C_5H_6Ag_2N_2O_6$ (%): C, 14.8; H, 1.5; N, 6.9. Found: C, 15.2; H, 1.4; N, 7.5. FTIR (KBr)/cm^{-1}: 3235, 1649, 1585, 1532, 1493, 1436, 1379, 1211, 1149, 1074, 948, 827, 802, 673, 631, 594, 510.

2.3. Adsorption experiments

Sulfamethoxazole (SMX), promethazine (PMH), anionic methyl orange (MO), cationic basic Brown 1 (BB-1), cationic methylene blue (MB) and cationic rhodamine B (RhB) were selected as model organic pollutants to evaluate the adsorption performance of **BUC-16**, as illustrated in Scheme S1. A solid sample (50 mg) of **BUC-16** was added to 200 mL of MO (10 mg L^{-1}), BB-1 (50 mg L^{-1}), MB (20 mg L^{-1}) and RhB (10 mg L^{-1}) aqueous solution in a 300 mL breaker, respectively. The mixtures were vibrated in water bath shaker with speed of 150 r min^{-1} at 293 K. Samples of 1.0 mL aliquots were extracted using a 0.45 μm syringe filter (Tianjin Jinteng) at regular intervals for analysis.

2.4. Antibacterial activity

Surface water samples collected from Minghu Lake at BUCEA campus were used to test the antibacterial ability and alga-inhibiting activity of BUC-16, following agar plate diffusion assay method described in previously published literature [12]. Two micrograms BUC-16 powders with particle size less than 0.1 mm were added to 200.0 mL surface water samples. After 4 h cultivation, the supernatant was vaccinated onto an Agar plate to observe the growth status of bacterial colonies. Antibacterial activity of **BUC-16** was further tested against *Escherichia coli* (CICC 23429) by determining the minimal inhibitory concentration (MIC), growth inhibition assay and zone of inhibition technique, respectively. All bacterial routine handlings were conducted with Luria Bertani (LB) broth at 37 ℃, and long-term storage was performed in glycerol stocks at −30 ℃. The medium was prepared by dissolving agar and LB broth in distilled water.

2.5. Zone of inhibition technique

The mixture of dissolved agar and LB broth was autoclaved for 15 min at 121 ℃ and then dispensed into sterilized Petri dishes, which was allowed to solidify and used for inoculation. The target microorganism cultures were prepared separately in 100 mL of liquid LB broth medium for activation. Activated strain (50 μL) was placed onto the surface of an agar plate and speeded evenly over the surface by means of a sterile bent glass rod. The neutral filters with diameter of 6 mm infiltrating **BUC-16** powders were put into each plate. The diameters of inhibition zones were determined by Vernier callipers, and all the data were the mean values of three parallel tests.

2.6. Minimum inhibitory concentration (MIC) and Growth inhibition assay

Bacteria were maintained in general LB liquid media and were shaken at 37 ℃ overnight. Diluted overnight bacterial and LB liquid cultures were handled with serial dilutions of **BUC-16** powders for 24 h while shaking at 37 ℃. Finally, the optical density was measured at 600 nm (OD_{600}) via UV–vis spectrometer to calculate the MIC value.

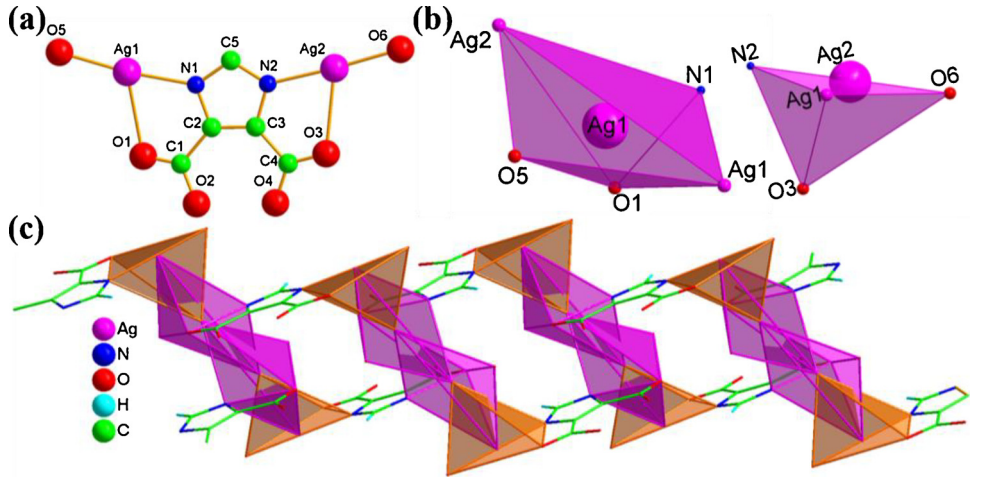

Fig. 1. (a) The coordination environment of the two crystallographically independent Ag(I) centers in **BUC-16**, and (b) Highlight of the coordination polyhedral for Ag1(I) and Ag2(I) ions, respectively. (c) The 1D infinite $[Ag_2(idca)(H_2O)_2]_n$ chains in **BUC-16**.

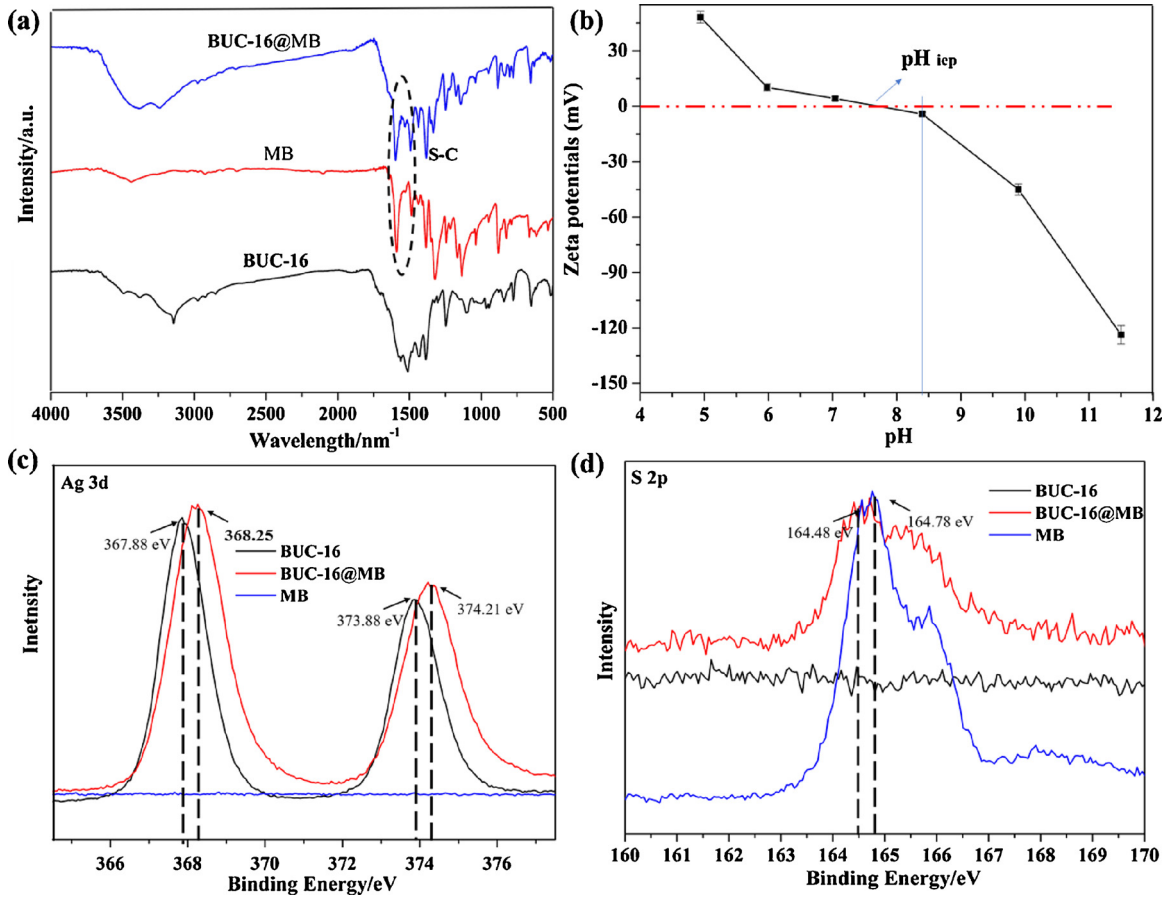

Fig. 2. (a) FTIR spectra of as-synthesized **BUC-16**, MB and **BUC-16** after absorbing MB. (b) The pH effect on the zeta potential of **BUC-16**. (c) XPS spectra for Ag 3d regions of **BUC-16** in the single and after MO adsorption. (d) XPS spectra for S 2p regions of **BUC-16** before and after MB adsorption.

Diluted bacteria and LB liquid cultures were treated with different amounts of **BUC-16** powder for 48 h while shaking at 37 °C, respectively. OD_{600} was determined with a UV–vis spectrometer at set time intervals to draw the growth curves of bacteria. The growth curve of *E. coli* without **BUC-16** as antibacterial agent was also measured as blank. All the data for OD_{600} were the average values of three parallel tests.

2.7. Direct method of quantification of silver release

The **BUC-16** powders were immersed in distilled water in 200 ppm for 5 d. The concentrations of released Ag^+ in the supernatant were determined by ICP-OES (ICAP 7000) every 4 h in the first day. And then, the concentration of released Ag^+ was monitored once a day.

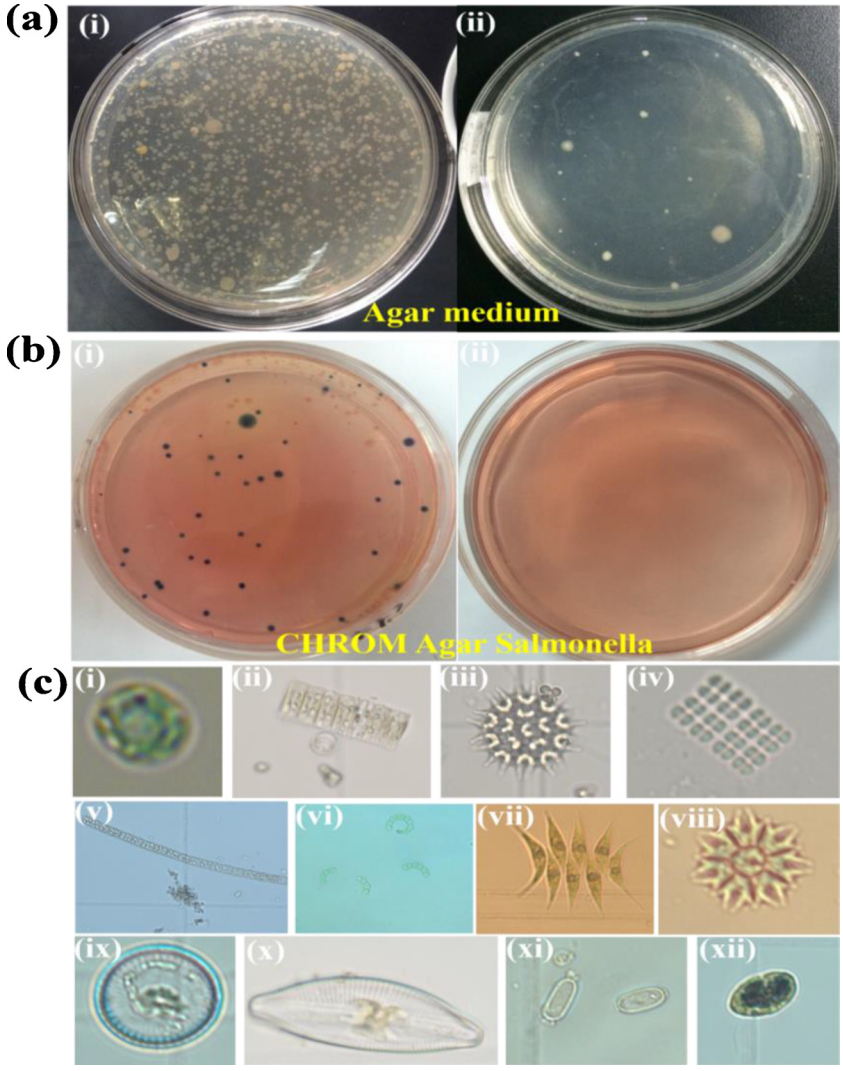

Fig. 3. Agar plate diffusion experiment to estimate antibacterial activity of **BUC-16** onto surface layer of lake water. (a_i) and (b_i) with the absence of **BUC-16**. (a_{ii}) and (b_{ii}) with the presence of **BUC-16**. (Incubation conditions: 310 K, 24 h). The alga observed in the water sample collected from Ming Lake in BUCEA campus: (c_i) Microcystis aeruginosa, (c_{ii}) Fragilariaceae, (c_{iii}) Pediastrum boryanum, (c_{iv}) Merismopedia, (c_v) Spirogyra, (c_{vi}) Anabeana, (c_{vii}) Scenedesmus dimorphus, (c_{viii}) Pediastrum duplex, (c_{ix}) Chlorella vulgaris, (c_x) Cmbella, (c_{xi}) Cocconeis, (c_{xii}) Euglena.

2.8. Alga cell cultures and counting

Cyanobacteria (Microcystis aeruginosa FACHB-905) were selected in this study, which was obtained from the Institute of Hydrobiology, Chinese Academy of Sciences. The cyanobacteria strains were cultured in BG-11 media [37], and were incubated at 25 °C under a constant light flux with a light/dark loop of 12 h/12 h. The strains were used for experiments once the exponential growth phase was reached, usually in 7–10 d. Cell counting for the M. aeruginosa strains was conducted with an Axio Imager A2 microscope (Carl Zeiss, Germany) [12]. Before cell counting, surface water samples collected from Minghu Lake at Beijing University of Civil Engineering and Architecture (BUCEA) in Beijing, China (hyperthermic aseptic water bath) was used to cultivate M. aeruginosa. One milliliter sample was extracted and placed under the Axio Imager A2. After being allowed to settle for 10 min, the samples were counted at 200× magnification.

2.9. The control of odour (β-cyclocitral) formed by M. aeruginosa

To test the application of **BUC-16** on odor control, two 200 mL water samples (the water qualities were listed in Table S8) collected from Minghu Lake in BUCEA campus was carried out heat sterilization. The cyanobacteria strains were cultured in one water sample with 2.0 mg **BUC-16** powder and in another water sample as blank. Two 2.0 mL solutions extracted from the above-stated two water samples with cultured cyanobacteria strains were transferred to headspace bottles with GF/C filter membrane filtration (Whatman), respectively, then 2.0 g NaCl solids were added, along with 10 μL 100 g L^{-1} IBMP (2-Methoxy-3-isobutyl pyrazine, 98%, Acros organics) was injected into as internal standard (Fig. S2). The odour compounds formed by Cyanobacteria were determined by headspace solid phase micro-extraction with gas chromatography combined with mass spectrometry (HSPME-GC–MS) [38–40]

2.10. In vitro cytotoxicity test

NIH-3T3 cells were maintained in Dulbecco's modified Eagle's medium (DMEM) containing 10% fetal bovine serum at 37 °C in a humidified atmosphere containing 5% CO_2 [41]. NIH-3T3 cells were incubated with primary antibody for 1 h at 4 °C, washed with PBS for three times. After repeatedly rinsed with PBS, the cells were observed by confocal laser scanning microscopy (CLSM, Nikon A1R, Japan). The cytotoxicity effect of **BUC-16** was investigated by MTT method according to the manufacturer's suggested procedures. NIH-3T3 cells were

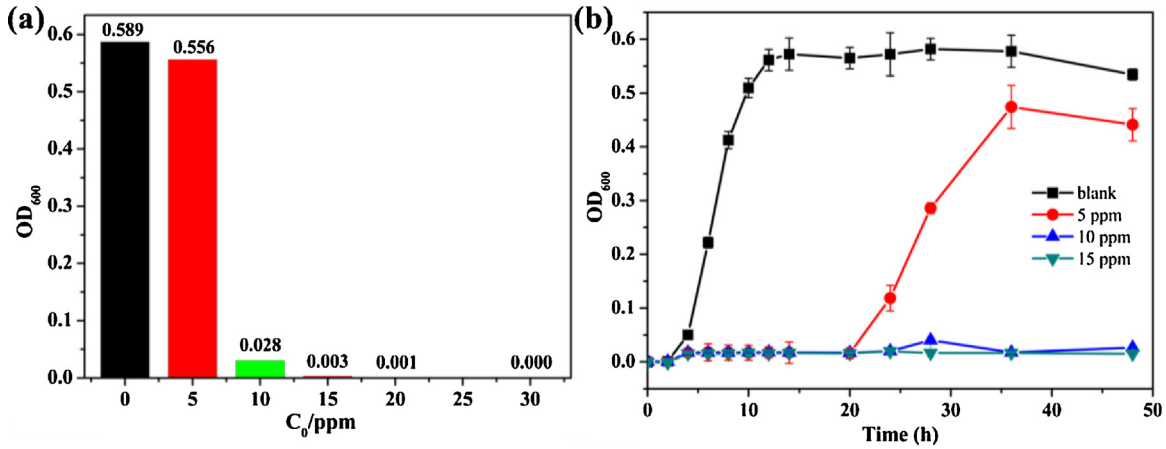

Fig. 4. (a) MIC of **BUC-16** against E. *coli* (Incubation conditions: 310 K, 36 h). (b) Growth curves of E. *coli* in different concentrations (0–15 ppm) of **BUC-16**.

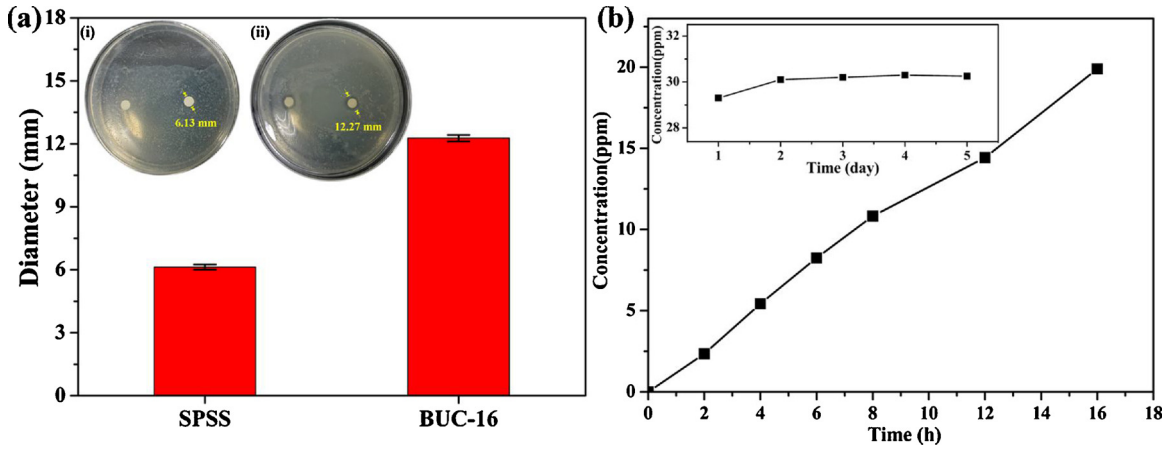

Fig. 5. (a) Images and diameters of inhibition zones (inset) for SPSS (i), **BUC-16**(ii) against E. *coli*. (b) Concentrations of released Ag^+ from **BUC-16** aqueous solution (16 h) and aqueous solution within 5 d (inset).

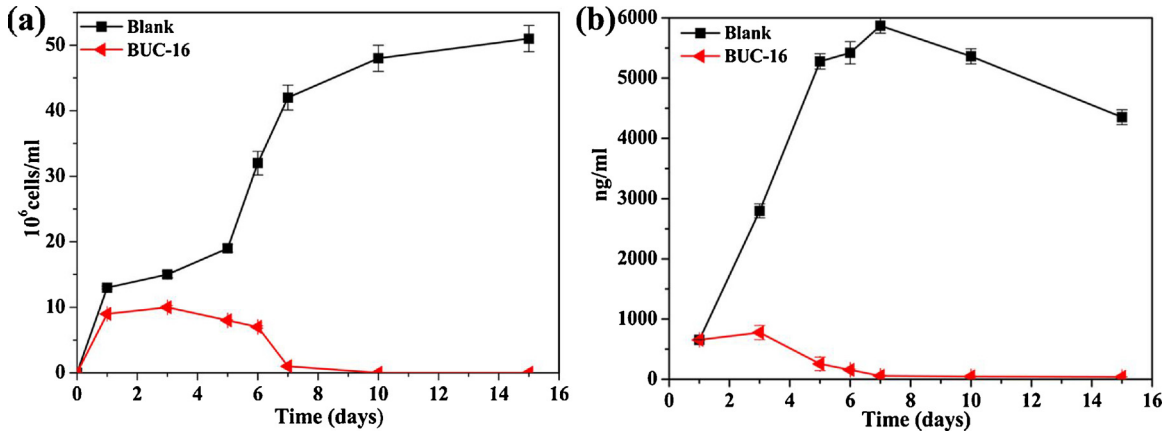

Fig. 6. (a) Growth curves of M. aeruginosa and (b) concentrations evolution of *β*-cyclocitral without and with **BUC-16** (2 mg BUC-16 in 200 mL aqueous solution).

treated with **BUC-16** or blank HSST micelles (as a control) for 48 h. The data are expressed as the percentage of surviving cells and are reported as the mean values of three parallel measurements.

3. Results and discussion

3.1. Structure description of $[Ag_2(idca)(H_2O)_2]$ (BUC-16)

In this study, a 1D coordination polymer, $[Ag_2(idca)(H_2O)_2]$ (**BUC-16**), was synthesized from the reaction between 4,5-imidazoledicarboxylic acid and $AgNO_3$ in ammonia solutions followed by slow evaporation. Single-crystal XRD analysis indicates two crystallographically non-identical Ag^+ atoms with different geometries in the crystal structure of **BUC-16**. The distorted tetragonal pyramid geometries of Ag1 atoms were completed by one oxygen atom from water molecule (Ag(1)···O(5) 2.141 Å), one oxygen atom from $idca^{2-}$ ligand (Ag(1) ···O(1) 2.630 Å), nitrogen atom from the same $idca^{2-}$ ligand (Ag(1) ···N(1) = 2.141 Å), Ag(1)#1 and Ag(2)#1 (Ag(1)-Ag(1)#1 = 2.9959(8) Å and Ag(1)-Ag(2)#2 = 3.0083(6) Å), which is comparable to those (2.97 (2)~ 3.42 (3) Å) found in other Ag coordination

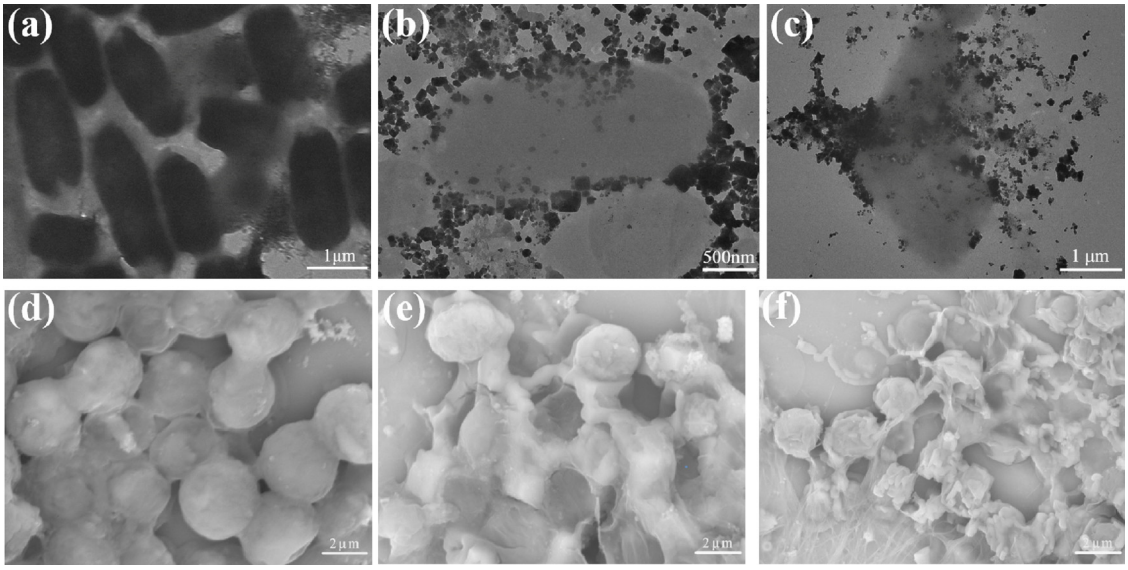

Fig. 7. TEM morphological images of *E. coli* cell structures: intact (a) and damaged by **BUC-16** 0.5 h (b) and 1 h (c). SEM Morphological images of M. aeruginosa cell structures: intact (d) and damaged by **BUC-16** (e) 2 h and (f) 4 h.

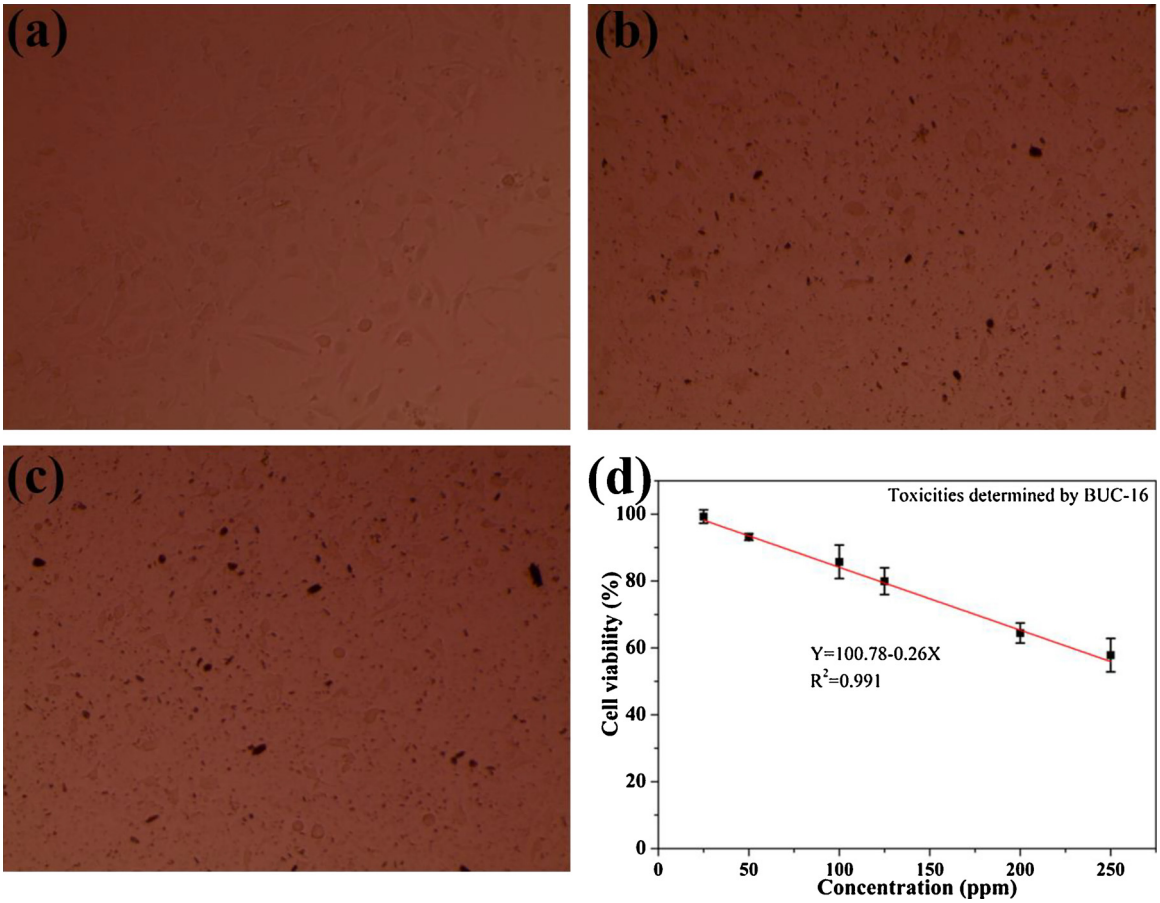

Fig. 8. Cytotoxicity assay against NIH-3T3 cells treated with **BUC-16**: (a) blank; (b) 25 ppm; (c) 50 ppm and (d) The concentration related cytotoxicity of **BUC-16** against NIT-3T3 cells after 48 h incubation.

polymers with imidazole-donor ligands [12,42]. The distorted square of Ag2 atom was coordinated by O3 (Ag(2)···O(3) = 2.608 Å) from $idca^{2-}$ ligands, O6 (Ag(2)···O(6) = 2.139 Å) from water molecules and N2 (Ag(2)-N(2) = 2.131) and Ag(1)#3 (Ag(2)-Ag(1)#3 = 3.0083 Å), as illustrated in Fig. 1 and Table S2. The infinite 1D $[Ag_2(idca)(H_2O)_2]_n$ chains join into 3D supramolecular framework via abundant hydrogen-bonding interactions, Ag···Ag interactions, and Ag···N interactions (Tables S1–S3). It was found that the as-prepared **BUC-16** is insoluble in water and common organic solvents. In addition, **BUC-16** is environmentally stable under air, light and in water, which was confirmed by powder XRD analysis as exhibited in Fig. S3. **BUC-16** has a positive surface charge from pH ranging from 5.0 to 7.5, while it becomes

negative at the pH range of 7.5–11.5.

3.2. Adsorption performances of BUC-16 toward organic pollutants

In order to explore the adsorption performance of **BUC-16** toward organic pollutants, adsorption experiments were carried out in batch system, in which some typical organic pollutants like sulfamethoxazole (SMX), promethazine hydrochlorine (PMH), anionic methyl orange (MO), cationic basic Brown 1 (BB-1), cationic methylene blue (MB) and cationic rhodamine B (RhB) (Scheme S1) were selected as target models. **BUC-16** exhibited good adsorption performance toward SMX, PMH, MB and BB-1, with maximum adsorption capacities of 1395, 675, 1317 and 339 mg g^{-1}, respectively. But, **BUC-16** was inert to anionic MO and cationic RhB with big molecular size, as illustrated in Fig. S4.

Considering that it is convenient to monitor the concentration of organic dye via colorimetry, MB was selected as organic pollutant model to investigate the adsorption performance, including adsorption kinetics [43], isotherm models and related thermodynamic parameters [44]. The pseudo-first-order model and the pseudo-second-order model had been often used to describe the adsorption kinetics processes. The calculated k_1 and k_2 values and the corresponding linear regression correlation coefficient (R^2) values of the above-stated two models were shown in Table S5. The obtained R^2 values for the pseudo-first-order model were above 0.99 at different concentrations, implying the pseudo-first-order model was more suitable to describe the related adsorption behavior. A good agreement with pseudo-first-order model was also confirmed by similar values of calculated q_e values and the experimental ones, as listed in Table S4.

To describe the equilibrium isotherms, the equilibrium data of MB adsorbing onto **BUC-16** at different temperature of 288 K, 293 K, 298 K, 303 K and 308 K were fitted with Langmuir, Freundlich, and Dubinin-Radushkevich (D–R), respectively. The higher coefficients R^2 of Langmuir equations ranging from 0.976 to 0.999 showed that Langmuir isotherm model preferred to describe the adsorption process [45], as listed in Table S6. As well, the q_{max} values obtained from Langmuir model increased with the increasing temperature, suggesting that the adsorption was favorable at higher temperature and the process was endothermic. The values of ΔG° decreased from −27.20 to −30.58 kJ mol^{-1} with the temperature from 288 K to 308 K, indicating that the adsorption process became more favorable at higher temperatures [46], as listed in Table S7. The negative values of ΔG° suggested that the sorption process may be controlled by both physical and chemical sorption [47]. The positive value of ΔH° (19.93 kJ mol^{-1}) indicated that the adsorption reaction between MB and **BUC-16** is endothermic, evidenced by the increase of adsorption capacity with temperature. [48] The positive value of ΔS° (164 J mol^{-1} K^{-1}) implied the increased randomness at the solid-solution interface and the affinity of MB onto **BUC-16** [1,49].

The adsorption of MB onto **BUC-16** was confirmed by FTIR, which presented the strong signals of characteristics C–S peaks of MB in FTIR spectra (Fig. 2a) [1]. Also, XPS was introduced to characterize the MB affinity onto **BUC-16**. As illustrated in Fig. 2(c) and (d), the strong XPS spectra signals of S element (the characteristics element of MB in this system) with binding energy of 164.78 eV could be observed. [50] Meanwhile, the XPS spectra show that the adsorption of MB by **BUC-16** led to a shift to lower energies for the S 2p peaks, from 164.78 eV to 164.48 eV (Fig. 2d). The XPS spectra show that Ag 3d peak splits into Ag 3d5/2 (367.88 eV) and Ag 3d3/2 (373.88 eV) due to spin orbit coupling and these peak positions match well with the reported values [51]. As well, the difference of 6.00 eV between the peaks matches well with the reported value of metallic silver [52,53]. The 0.36 eV energy shift for the Ag peaks was attributed to the interaction between the S element of MB and the Ag^+ ion. The weak interactions (π-π stacking) between the imidazole rings of **BUC-16** and the aromatic rings of MB might contribute to its remarkable adsorption performance towards MB [54–56].

3.3. Anti-microbial activity and odour control

The results of the agar plate diffusion assay experiment [57] revealed that the number of bacterial colonies was 9880 CFU mL^{-1} 103 CFU mL^{-1} without and with **BUC-16**, respectively, as illustrated in the Fig. 3 and Fig. S5. In detail, **BUC-16** could efficiently inhibit the growth of Enterobacter cloacae, salmonella, *Citrobacter* and so on, as listed in Fig. 3a, b and Table S9. The algae in the water sample are observed with the aid of the ZEISS Axio Imager A2, the results revealed that **BUC-16** could efficiently inhibit the growth of Microcystis aeruginosa, fragilariaceae, pediastrum boryanum, merismopedia and so on, as listed in Fig. 3c and Video 2, implying that **BUC-16** exhibited remarkable alga-inhibiting properties.

Gram-negative bacteria (E. *coli*) was selected as model microorganism to evaluate the antibacterial activity of **BUC-16**, in which the minimum inhibitory concentration (MICs) determined using an optical density method [53] of **BUC-16** against E. *coli* were in the range of 5–10 ppm (Fig. 4a and Fig. S4). It revealed that **BUC-16** exhibited higher antibacterial activities than most of commonly used silver-based compounds in previous reports [12,54]. The inhibitory effect on the growth of E. *coli* for **BUC-16** in 10 ppm exhibited its long-term bacteriostatic activity (48 h) in Fig. 4b and Fig. S10b. Additionally, the diameter of the inhibition zone emerged from **BUC-16** (12.27 mm) (Fig. 5a) was much bigger than that of stroke-physiological saline solution (SPSS, 6 mm), further confirming the superior antimicrobial activity of **BUC-16**.

BUC-16 also exhibited good odor (β-cyclocitral) control activity, in which the microcystis aeruginosa (M. aeruginosa FACHB-905) was selected as the representative microorganism. Two micrograms **BUC-16** powders with particle size less than 0.1 mm were added to 200 mL surface water sample. As shown in Fig. 6, the inhibition of M. aeruginosa with the presence of **BUC-16** occurred after 6th day, and the concentration of β-cyclocitral decreased from the 3rd day. It was worthy to noting that nearly no M. aeruginosa cells and no β-cyclocitral can be detected after the 7th day. While, the β-cyclocitral concentration increased to 2000–5000 ng mL^{-1} from 3rd day to 7th day.

To understand the inhabitation mechanism of **BUC-16** on the growth of *E. coli* and M. aeruginosa, transmission electron microscope (TEM) and scanning electron microscope (SEM) were used to observe the morphological changes of the cells [12]. As illustrated in Fig. 7(a) and (d), intact *E. coli* and M. aeruginosa had distinct outer membranes, implying that their cell structures were well preserved even under high vacuum and energy electron beam. However, after being exposed to **BUC-16**, both E. *coli* and M. aeruginosa lost their cellular cohesion with their outer membranes being seriously destroyed, resulting in the cells' cytoplasm outflow, and finally death [11,63,64], as illustrated in Fig. 7, Figs. S6 and S7. It is believed that the slow release of Ag^+ ion of **BUC-16** could provide steady and prolonged Ag^+ ions in aqueous solution, which could account for its outstanding antibacterial and odor controlling performances. The previous studies have revealed that the release of Ag^+ ions of Ag-based materials can lead to their antibacterial activities [12,58,59]. In this study, the Ag^+ released from **BUC-16** was determined by ICP-OES, with the Ag^+ concentration progressively increased in the first day followed by slow increases at the 2nd day, then maintained at a stable level with average Ag^+ concentration being ca. 30 ppm for 3–5 d, as illustrated in Fig. 5b.

Based on our experimental results and previous research [12], a possible antibacterial and odour control mechanism of **BUC-16** could be understood as follows. The **BUC-16** particles could diffuse on the *E. coli* and M. aeruginosa surface, and release Ag^+ ions resulted in the change of ion balance and destroyed ion channels [12,60,61]. It was deemed that the fine **BUC-16** particles can also penetrate into the bacteria to wreck the cells by interaction with lipotropic acid or hydroxyl groups of peptidoglycan membranes, as well as phosphate groups of phosphonolipid membranes [62]. Furthermore, the slowly-released Ag^+ ions might interact with the R—SH groups of proteins to impact the bacterial

membrane's integrity and permeability [63]. Finally, the outflow of the cytoplasm resulted from the rupture of the cell membrane caused the death of the E. *coli* and M. aeruginosa.

3.4. In vitro cytotoxicity test

NIH-3T3 cells were selected as targeted cells to test the cell toxicity of **BUC-16** with MTT method [41]. After 48 h incubation, the killing effect of **BUC-16** for NIH-3T3 cells was showed in Fig. 8. A fairly weak dose-dependence can be observed with the MIC of **BUC-16** against E. *coli* was only 5–10 ppm [64], even though higher killing effect for NIH-3T3 cells and IC50 can be achieved with the concentration of **BUC-16** above ~200 ppm. For example, viability of NIH-3T3 cells was still over 90% with presence of 50 ppm **BUC-16** even after 48 h incubation, as showed in Fig. 8d, suggesting that the **BUC-16** has a reasonable biocompatibility.

4. Conclusion

In all, $[Ag_2(idca)(H_2O)_2]$ (BUC-16) was synthesized and used as an adsorbent to adsorb organic pollutants promethazine hydrochlorine, sulfamethoxazole, methylene blue. The adsorption process followed a pseudo-second-order kinetic model and fitted well with the Langmuir isotherm. The controllable slow-release of Ag^+ ions from **BUC-16** resulted into its outstanding antimicrobial and alga-inhibiting performance toward Gram-negative bacteria E. *coli* and M. aeruginosa. **BUC-16** can be used to remove unpleasant odor like *β*-cyclocitral via its alga-inhibiting activity. As far as we know, it is the first study on alga-inhibiting properties of coordination polymer. Furthermore, **BUC-16** exhibit good biocompatibility and potentially safe to human being and environment. Further studies are underway to verify that coordination polymers are safe and effective materials for aquatic ecosystem.

Conflict of interest

None.

Acknowledgments

The authors acknowledge the financial support from Great Wall Scholars Training Program Project of Beijing Municipality Universities (CIT&TCD20180323), Project of Construction of Innovation Teams and Teacher Career Development for Universities and Colleges Under Beijing Municipality (IDHT20170508), Beijing Postdoctoral Research Foundation, Beijing Talent Project (2017A38) and the Fundamental Research Funds for Beijing Universities (X18075/X18076). The in-vitro cytotoxicity test was conducted at Beijing University of Chemical Technology.

Appendix A. Supplementary data

Supplementary material related to this article can be found, in the online version, at doi:https://doi.org/10.1016/j.jece.2018.07.035.

References

[1] Y.Q. Zhang, C. Wang, T. Zhu, P. Wang, S.J. Gao, Ultra-high uptake and selective adsorption of organic dyes with a novel polyoxomolybdate-based organic-inorganic hybrid compound, RSC Adv. 5 (2015) 45688–45692.
[2] G. Férey, Hybrid porous solids: past, present, future, Chem. Soc. Rev. 37 (2008) 191–214.
[3] S. Kitagawa, R. Matsuda, Chemistry of coordination space of porous coordination polymers, Coord. Chem. Rev. 251 (2007) 2490–2509.
[4] S. Sorribas, B. Zornoza, C. Téllez, J. Coronas, Ordered mesoporous silica-(ZIF-8) core-shell spheres, Chem. Commun. 48 (2012) 9388–9390.
[5] J. Lee, O.K. Farha, J. Roberts, K.A. Scheidt, S.T. Nguyen, J.T. Hupp, Metal–organic framework materials as catalysts, Chem. Soc. Rev. 38 (2009) 1450–1459.
[6] F.X. Wang, X.H. Yi, C.C. Wang, J.G. Deng, Photocatalytic Cr(VI) reduction and organic-pollutant degradation in a stable 2D coordination polymer, Chin. J. Catal. 38 (2017) 2141–2149.
[7] C.C. Wang, X.D. Du, J. Li, X.X. Guo, P. Wang, J. Zhang, Photocatalytic Cr(VI) reduction in metal-organic frameworks: a mini-review, Appl. Catal. B 193 (2016) 198–216.
[8] C.C. Wang, Y.Q. Zhang, T. Zhu, P. Wang, S.J. Gao, Photocatalytic degradation of methylene blue and methyl orange in a Zn(II)-based Metal–Organic Framework, Desalin. Water Treat. 33 (2015) 885–896.
[9] H.P. Jing, C.C. Wang, Y.W. Zhang, P. Wang, R. Li, Photocatalytic degradation of methylene blue in ZIF-8, RSC Adv. 4 (2014) 54454–54462.
[10] C.C. Wang, J.R. Li, X.L. Lv, Y.Q. Zhang, G. Guo, Photocatalytic organic pollutants degradation in metal–organic frameworks, Energy Environ. Sci. 7 (2014) 2831–2867.
[11] G. Wyszogrodzka, B. Marszałek, B. Gil, P. Dorożyński, Metal-organic frameworks: mechanisms of antibacterial action and potential applications, Drug Discov. Today 21 (2016) 1009–1018.
[12] A. Liu, C.-C. Wang, C.-Z. Wang, H.-f. Fu, W. Peng, Y.-L. Cao, H.-Y. Chu, A.-F. Du, Selective adsorption activities toward organic dyes and antibacterial performance of silver-based coordination polymers, J. Colloid Interface Sci. 512 (2018) 730–739.
[13] H. Li, M. Eddaoudi, M. O'Keeffe, O.M. Yaghi, Design and synthesis of an exceptionally stable and highly porous metal-organic framework, Nature 402 (1999) 276–279.
[14] J.-R. Li, R.J. Kuppler, H.-C. Zhou, Selective gas adsorption and separation in metal–organic frameworks, Chem. Soc. Rev. 38 (2009) 1477–1504.
[15] J. Zhang, C.-C. Wang, P. Wang, Y.-L. Cao, Selective uptake of organic dyes in a silver-based coordination polymer, RSC Adv. 6 (2016) 73595–73599.
[16] X.D. Du, C.C. Wang, J.G. Liu, X.D. Zhao, J. Zhong, Y.X. Li, J. Li, P. Wang, Extensive and selective adsorption of ZIF-67 towards organic dyes: performance and mechanism, J. Colloid Interface Sci. 506 (2017) 437–441.
[17] J.-J. Li, C.-C. Wang, H.-f. Fu, J.-R. Cui, P. Xu, J. Guo, J.-R. Li, High-performance adsorption and separation of anionic dyes in water using a chemically stable graphene-like metal-organic framework, Dalton Trans. 46 (2017) 10197–10201.
[18] X.D. Du, C.C. Wang, J. Zhong, J.G. Liu, Y.X. Li, P. Wang, Highly efficient removal of Pb^{2+} by a polyoxomolybdate-based organic-inorganic hybrid material {(4-Hap)$_4$[Mo_8O_{26}]}, J. Environ. Chem. Eng. 5 (2017) 1866–1873.
[19] B. Gole, A.K. Bar, P.S. Mukherjee, Fluorescent metal-organic framework for selective sensing of nitroaromatic explosives, Chem. Commun. 47 (2011) 12137–12139.
[20] W.J. Li, J. Lu, S.Y. Gao, Q.H. Li, R. Cao, Electrochemical preparation of metal-organic framework films for fast detection of nitro explosives, J. Mater. Chem. A 2 (2014) 19473–19478.
[21] L. Sorace, C. Benelli, D. Gatteschi, Lanthanides in molecular magnetism: old tools in a new field, Chem. Soc. Rev. 40 (2011) 3092–3104.
[22] K.M. Taylor-Pashow, J.D. Rocca, Z. Xie, S. Tran, W. Lin, Postsynthetic modifications of iron-carboxylate nanoscale metal–organic frameworks for imaging and drug delivery, J. Am. Chem. Soc. 131 (2009) 14261–14263.
[23] H. Fu, Z. Wang, X. Wang, P. Wang, C.-C. Wang, Formation mechanism of rod-like ZIF-L and fast phase transformation from ZIF-L to ZIF-8 with morphology changes controlled by polyvinylpyrrolidone and ethanol, CrystEngComm 20 (2018) 1473–1477.
[24] C.-C. Wang, Y.-S. Ho, Research trend of metal–organic frameworks: a bibliometric analysis, Scientometrics 109 (2016) 481–513.
[25] N.A. Khan, Z. Hasan, S.H. Jhung, Adsorptive removal of hazardous materials using metal-organic frameworks (MOFs): a review, J. Hazard. Mater. 244–245 (2013) 444.
[26] Q.R. Fang, D.Q. Yuan, J. Sculley, J.R. Li, Z.B. Han, H.C. Zhou, Functional mesoporous metal – Organic frameworks for the capture of heavy metal ions and size-selective catalysis, Inorg. Chem. 49 (2010) 11637–11642.
[27] K.A. Cychosz, A.G. Wong-Foy, A.J. Matzger, Liquid phase adsorption by microporous coordination polymers: removal of organosulfur compounds, J. Am. Chem. Soc. 130 (2008) 6938–6939.
[28] M.R. Azhar, H.R. Abid, H. Sun, V. Periasamy, M.O. Tadé, S. Wang, Excellent performance of copper based metal organic framework in adsorptive removal of toxic sulfonamide antibiotics from wastewater, J. Colloid Interface Sci. 478 (2016) 344–352.
[29] X. Zhao, Y. Wei, H. Zhao, Z. Gao, Y. Zhang, L. Zhi, Y. Wang, H. Huang, Functionalized metal-organic frameworks for effective removal of rocephin in aqueous solutions, J. Colloid Interface Sci. 514 (2017) 234–239.
[30] Y. Peng, Y. Zhang, H. Huang, C. Zhong, Flexibility induced high-performance MOF-based adsorbent for nitroimidazole antibiotics capture, Chem. Eng. J. 333 (2018) 678–685.
[31] X.-Y. Xu, C. Chu, H. Fu, X.-D. Du, P. Wang, W. Zheng, C.-C. Wang, Light-responsive UiO-66-NH2/Ag3PO4 MOF-nanoparticle composites for the capture and release of sulfamethoxazole, Chem. Eng. J. 350 (2018) 436–444.
[32] Y. Li, Z. Yang, Y. Wang, Z. Bai, T. Zheng, X. Dai, S. Liu, D. Gui, W. Liu, M. Chen, L. Chen, J. Diwu, L. Zhu, R. Zhou, Z. Chai, T.E. Albrecht-Schmitt, S. Wang, A mesoporous cationic thorium-organic framework that rapidly traps anionic persistent organic pollutants, Nat. Commun. 8 (2017) 1354.
[33] X. Lu, J. Ye, Y. Sun, R.F. Bogale, L. Zhao, P. Tian, G. Ning, Ligand effects on the structural dimensionality and antibacterial activities of silver-based coordination polymers, Dalton Trans. 43 (2014) 10104–10113.
[34] Bruker AXS, SMART, Version 5.611, Bruker AXS, Madison, WI, USA, 2000.
[35] Bruker AXS, SAINT, Version 6.28, Bruker AXS, Madison, WI, USA, 2003.
[36] M.D. Yuuki Shiomi, S. Nishiumi, M.D. Makoto Ooi, N. Hatano M.S.M. PhD, M.D. Tomoo Yoshie, M.D. Yasuyuki Kondo, M.D. Keisuke Furumatsu, M.D. Hideyuki Shiomi H.K.M. PhD, GC–MS-based metabolomic study in mice with colitis induced by dextran sulfate sodium, Inflamm. Bowel Dis. 17 (2011)

2261–2274.
[37] R. Rippka, J. Deruelles, J.B. Waterbury, M. Herdman, R.Y. Stanier, Generic assignments, strain histories and properties of pure cultures of Cyanobacteria, J. Gen. Microbiol. 111 (1979) 1–61.
[38] Y. Zuo, L. Li, T. Zhang, L. Zheng, G. Dai, L. Liu, L. Song, Contribution of Streptomyces in sediment to earthy odor in the overlying water in Xionghe Reservoir, China, Water Res. 44 (2010) 6085–6094.
[39] X. Deng, G. Liang, J. Chen, M. Qi, P. Xie, Simultaneous determination of eight common odors in natural water body using automatic purge and trap coupled to gas chromatography with mass spectrometry, J. Chromatogr. A 1218 (2011) 3791–3798.
[40] M. Kang, N.Z. Jin, Z. Min, Y.J. He, M. Kang, N.Z. Jin, Z. Min, Y.J. He, Accurate analysis of trace earthy-musty odorants in water by headspace solid phase microextraction gas chromatography–mass spectrometry, J. Sep. Sci. 35 (2012) 1494–1501.
[41] C. Zhu, H. Zhang, W. Li, L. Luo, X. Guo, Z. Wang, F. Kong, Q. Li, J. Yang, Y. Du, Suppress orthotopic colon cancer and its metastasis through exact targeting and highly selective drug release by a smart nanomicelle, Biomaterials 161 (2018) 144–153.
[42] P.J. Steel, C.M. Fitchett, Metallosupramolecular silver(I) assemblies based on pyrazine and related ligands, Coord. Chem. Rev. 252 (2008) 990–1006.
[43] Y.S. Ho, G. Mckay, Kinetic model for lead(II) sorption on to peat, Adsorpt. Sci. Technol. 16 (1998) 243–255.
[44] N.A. Khan, J.W. Jun, J.H. Jeong, S.H. Jhung, Remarkable adsorptive performance of a metal-organic framework, vanadium-benzenedicarboxylate (MIL-47), for benzothiophene, Chem. Commun. 47 (2011) 1306–1308.
[45] S. Lin, Z. Song, G. Che, A. Ren, P. Li, C. Liu, J. Zhang, Adsorption behavior of metal–organic frameworks for methylene blue from aqueous solution, Microporous Mesoporous Mater. 193 (2014) 27–34.
[46] A. Zaki, M. El-Sheikh, J. Evans, S. El-Safty, Kinetics and mechanism of the sorption of some aromatic amines onto amberlite IRA-904 anion-exchange resin, J. Colloid Interface Sci. 221 (2000) 58–63.
[47] X.-G. Chen, S.-S. Lv, S.-T. Liu, P.-P. Zhang, A.-B. Zhang, J. Sun, Y. Ye, Adsorption of methylene blue by rice hull ash, Sep. Sci. Technol. 47 (2012) 147–156.
[48] A. Mittal, D. Jhare, J. Mittal, Adsorption of hazardous dye Eosin Yellow from aqueous solution onto waste material De-oiled Soya: isotherm, kinetics and bulk removal, J. Mol. Liq. 179 (2013) 133–140.
[49] M. Tong, D. Liu, Q. Yang, S. Devautour-Vinot, G. Maurin, C. Zhong, Influence of the framework metal ions on the dye capture behavior of the MIL-100 (Fe, Cr) MOF type solids, J. Mater. Chem. A 1 (2013) 8534–8537.
[50] B.J. Lindberg, K. Hamrin, G. Johansson, U. Gelius, A. Fahlman, C. Nordling, K. Siegbahn, Molecular spectroscopy by means of ESCA II. sulfur compounds. Correlation of electron binding energy with structure, Phys. Scr. 1 (1970) 286.
[51] M.F. Alkuhaili, Characterization of thin films produced by the thermal evaporation of silver oxide, J. Phys. D Appl. Phys. 40 (2007) 2847–2853.
[52] E. Filippo, A. Serra, D. Manno, Poly(vinyl alcohol) capped silver nanoparticles as localized surface plasmon resonance-based hydrogen peroxide sensor, Sens. Actuators B Chem. 138 (2009) 625–630.
[53] M. Banerjee, P. Sachdev, G.S. Mukherjee, Preparation of PVA/Co/Ag film and evaluation of its magnetic and microstructural properties, J. Appl. Phys. 111 (2012) 2061–2063.
[54] T. Shen, J. Luo, S. Zhang, X. Luo, Hierarchically mesostructured MIL-101 metal–organic frameworks with different mineralizing agents for adsorptive removal of methyl orange and methylene blue from aqueous solution, J. Environ. Chem. Eng. 3 (2014) 1372–1383.
[55] J. Ma, F. Yu, L. Zhou, L. Jin, M. Yang, J. Luan, Y. Tang, H. Fan, Z. Yuan, J. Chen, Enhanced adsorptive removal of methyl orange and methylene blue from aqueous solution by alkali-activated multiwalled carbon nanotubes, ACS Appl. Mater. Interfaces 4 (2012) 5749–5760.
[56] N.A. Khan, S.H. Jhung, Low-temperature loading of Cu^+ species over porous metal-organic frameworks (MOFs) and adsorptive desulfurization with Cu^+-loaded MOFs, J. Hazard. Mater. 237–238 (2012) 180–185.
[57] K.R. Fiebelkorn, S.A. Crawford, M.L. McElmeel, J.H. Jorgensen, Practical disk diffusion method for detection of inducible clindamycin resistance in Staphylococcus aureus and coagulase-negative Staphylococci, J. Clin. Microbiol. 41 (2003) 4740–4744.
[58] X. Lu, J. Ye, D. Zhang, R. Xie, R.F. Bogale, Y. Sun, L. Zhao, Q. Zhao, G. Ning, Silver carboxylate metal–organic frameworks with highly antibacterial activity and biocompatibility, J. Inorg. Biochem. 138 (2014) 114–121.
[59] W. Zhang, Y. Yao, N. Sullivan, Y. Chen, Modeling the primary size effects of citrate-coated silver nanoparticles on their ion release kinetics, Environ. Sci. Technol. 45 (2011) 4422–4428.
[60] Edyta Kopera, Tanja Schwerdtle, A. Andrea Hartwig, Wojciech Bal, Co(II) and Cd (II) substitute for Zn(II) in the zinc finger derived from the DNA repair protein XPA, demonstrating a variety of potential mechanisms of toxicity, Chem. Res. Toxicol. 17 (2004) 1452–1458.
[61] L. Thornton, V. Dixit, L.O. Assad, T.P. Ribeiro, D.D. Queiroz, A. Kellett, A. Casey, J. Colleran, M.D. Pereira, G. Rochford, Water-soluble and photo-stable silver(I) dicarboxylate complexes containing 1,10-phenanthroline ligands: antimicrobial and anticancer chemotherapeutic potential, DNA interactions and antioxidant activity, J. Inorg. Biochem. 159 (2016) 120–132.
[62] S. Medici, M. Peana, G. Crisponi, V.M. Nurchi, J.I. Lachowicz, M. Remelli, M.A. Zoroddu, Silver coordination compounds: a new horizon in medicine, Coord. Chem. Rev. 327–328 (2016) 349–359.
[63] Y. Matsumura, K. Yoshikata, S. Kunisaki, T. Tsuchido, Mode of bactericidal action of silver zeolite and its comparison with that of silver nitrate, Appl. Environ. Microbiol. 69 (2003) 4278–4281.
[64] T. Shen, X. Xu, L. Guo, H. Tang, T. Diao, Z. Gan, G. Zhang, Q. Yu, Efficient tumor accumulation, penetration and tumor growth inhibition achieved by polymer therapeutics: the effect of polymer architectures, Biomacromolecules 18 (2016) 217–230.